Constraining the Redshift Dependence of the CMB Temperature using the Sunyaev-Zeldovich Effect

Martin Nord
Chalmers University of Technology

Advisor: Cathy Horellou
Onsala Space Observatory

May 31, 2005

Abstract

Recent data have put powerful constraints on the present temperature of the cosmic microwave background (CMB) radiation, but the standard cosmological temperature-redshift relation, $T = T_0(1 + z)$, remains practically unverified. The Sunyaev-Zeldovich (SZ) effect is a promising candidate for placing constraints on $T(z)$, the former exhibiting a slight z dependence for all non-standard models. We discuss the possibility of using ratios of CMB intensity distortions due to the SZ effect at different radio frequencies to determine the correct relation. Mock SZ observations on simulated data for a fiducial ΛCDM cosmology are used in testing how well high-frequency data from the Planck satellite will be able to constrain $T(z)$. For a parameterization of the form $T = T_0(1+z)^{1-a}$, where $a = 0$ corresponds to the standard relation, we find that we can recover a to an accuracy of 10^{-3} at the 95% confidence level.

Acknowledgments

Part of this work has been carried out in collaboration with Daniel Johansson at Chalmers University of Technology. Daniel has also offered a lot of help with the manuscript, and brought coffee in times of need. Conversations with Anna Lévy on the topics of section 2 are gratefully acknowledged. A big thanks to Cathy Horellou for always offering help with the thesis work, and for introducing me to the marvels of cosmology. Thanks also to Gabriel Milewski for helping with pointers and other obscure aspects of programming. Last but not least, Martin Larsson deserves to be mentioned. Always into the bananas, always an inspiration, and always possessing great ideas in the kitchen.

Contents

1 Introduction

The current temperature of the cosmic microwave background radiation (CMB) has been measured with unprecedented accuracy by the Far Infrared Absolute Spectrometer (FIRAS) instrument on board the *COBE* (Cosmic Background Explorer) satellite, and the expected blackbody spectrum of this relic from the early universe has been demonstrated beyond doubt. In the standard Big Bang cosmology, the current temperature T_0 of the background radiation is related to the CMB temperature T at redshift z by

$$T(z) = T_0(1+z), \tag{1.1}$$

implicitly assuming that the blackbody spectrum is preserved in the redshifting of the CMB photons. This seemingly simple relation is derived in appendix A. It should be stressed that the results from FIRAS can only be applied to the CMB temperature and blackbody spectrum today, leaving the temperature at redshift z virtually unconstrained by the data.

In the present analysis, we shall look at non-standard forms of the temperature-redshift relation, and a way of constraining $T(z)$ using the Sunyaev-Zeldovich (henceforth SZ) effect, a distortion of the CMB spectrum in the direction of a galaxy cluster (the effect will be discussed in some detail in section 2). The redshift dependence of the SZ effect vanishes in the case of (1.1), but for any other $T(z)$ there will be a notable dependence. Unfortunately, the effect also depends on intrinsic cluster properties, such as the peculiar velocity and the electron temperature of the intracluster gas, making it rather difficult to determine the CMB temperature at the redshift of a particular cluster. However, using a large sample of clusters, this problem can be eliminated.

Data consistent with (1.1) have been presented by numerous authors, but so far only with large error bars. Population ratios derived from absorption lines from high-redshift quasars (e.g. Ge, Bechtold & Black 1997) can in general only yield upper limits on $T(z)$, because other processes could contribute to the excitation of atoms and molecules. Battistelli et al. (2002) illustrate how the relation can be constrained more effectively using the SZ effect, in this case applied to only two galaxy clusters. The Planck satellite, to be launched in 2007 by the European Space Agency, will conduct a full-sky SZE survey, making it possible to obtain much more restrictive bounds on the CMB temperature using this method. We will here expand on the method and apply it to simulated measurements like those to be carried out by the Planck high-frequency instrument.

Considering the near-perfect blackbody spectrum of the CMB today, arguments for a non-standard $T-z$ relation may seem far-fetched, especially in light of the fact that a non-linear relation will not preserve the blackbody shape of the spectrum unless secondary assumptions about the vacuum through which the photons propagate are made. Nonetheless, showing that (1.1) is really the case will strengthen the foundations of the Big Bang cosmology and the Friedman-Robertson-Walker metric. We seek not to introduce any new physics here; merely to rule out, if possible, models differing from (1.1).

We need to parameterize the temperature-redshift relation in such a way that deviations from the standard relation can be studied. For small deviations, assuming the standard relation is close to the right one (or indeed, *is* the right one), the parameterization is not of immediate importance to our general discussion. We shall use the form discussed by Lima et al. (2000), namely

$$T(z) = T_0(1+z)^{1-a}, \tag{1.2}$$

where $a \ll 1$ is a dimensionless parameter. For $a = 0$, we obtain the standard relation. This form is not merely a matter of convenience, but is derived on the basis of a plausible, though perhaps unlikely, thermodynamic cosmological scenario. The parameter a is constrained by

$$0 \leq a \leq 1$$

from theoretical considerations, and further constrained by previous observations (e.g. LoSecco et al. 2001) making it likely smaller than about 0.2.

To see how well the Planck mission will be able to constrain the free parameter, we first need to simulate the yield of the survey, which amounts to modeling the dark matter distribution of the universe. In this process, which is described in section 3, we will assume the standard temperature-redshift relation, implying that it will be inconsistent to make a significantly different from zero when simulating and fitting to mock SZ signals (section 4). Moreover, the SZ effect is derived on the basis of a blackbody spectrum, and it would be preposterous to assume that the blackbody we see today derives from a non-blackbody in the past. We must therefore assume the CMB is *always* a blackbody, which in the case of $a \neq 0$ implies that the number of photons is not conserved throughout the expansion (e.g. Ratra & Peebles 1988).

The CMB power spectrum yields powerful evidence that the universe is flat or very close to flat (e.g. Spergel et al. 2003), and the Supernova project (e.g. Perlmutter et al. 1999, Knop et al. 2003) has given strong limits on the contributions to the energy density from cold dark matter and the vacuum. For our simulation we will consider a fiducial ΛCDM cosmology with (Ω_M, Ω_Λ, h, σ_8) = (0.3, 0.7, 0.7, 0.9). Although changing these parameters has dramatic effects on the mass function and the number of observable galaxy clusters (dark matter halos), we can easily modify the yield of our mock observations at the end. The particular choice of cosmology thus has little bearing on our final results, and will for the most part not affect our general discussion.

2 The Sunyaev-Zeldovich Effect

2.1 The Non-Relativistic Diffusion Approximation

The Sunyaev-Zeldovich effect is the inverse Compton scattering of the CMB on hot ionized gas in galaxy clusters, causing a change in the apparent brightness of the radiation and a displacement of the spectrum toward the Rayleigh-Jeans regime. To a

first approximation, the effect can be computed from the Kompaneets equation (Zeldovich & Sunyaev 1969, Sunyaev & Zeldovich 1970b, 1972a), which gives the change in radiation intensity across the spectrum as

$$\Delta I = \frac{2(k_B T_0)^3}{h^2 c^2} \frac{k_B T_e}{m_e c^2} f(x) \tau_T, \tag{2.1}$$

where τ_T and T_e are the optical depth and the electron temperature of the intracluster gas, k_B, h and c are the Boltzmann and Planck constants and the speed of light in vacuum, respectively, m_e is the electron rest mass, and

$$f(x) \equiv \frac{x^4 e^x}{(e^x - 1)^2} \left(x \frac{e^x + 1}{e^x - 1} - 4 \right) \tag{2.2}$$

is the spectral shape factor with the dimensionless frequency

$$x \equiv \frac{h\nu}{k_B T(z)} (1 + z)$$

at (dimensional) frequency ν. In the case of the standard temperature-redshift relation, the z dependence vanishes so that

$$x = \frac{h\nu}{k_B T_0},$$

and in the case of the parameterization (1.2) we shall have

$$x = \frac{h\nu}{k_B T_0} (1 + z)^a. \tag{2.3}$$

Equation (2.1) is derived in appendix B.

Aside from the thermal effect on the CMB photons, the motion of a cluster with respect to the rest frame of the CMB will result in an additional change of the radiation intensity. For a cluster moving at velocity v_r, this kinematic effect is given by (Sunyaev & Zeldovich 1980a)

$$\Delta I_k = -\frac{2(k_B T_0)^3}{(hc)^2} \frac{x^4 e^x}{(e^x - 1)^2} \frac{v_r}{c} \tau_T, \tag{2.4}$$

where the sign convention is such that a receding cluster has a positive v_r. Assuming the effects are small, ΔI and ΔI_k can be added linearly. This convention will be used for the remainder of the paper.

Figure 1 shows the effect of the SZ effect on the blackbody spectrum of the CMB. Because of the small magnitude of the effect, it has to be magnified by a large factor to be seen clearly.

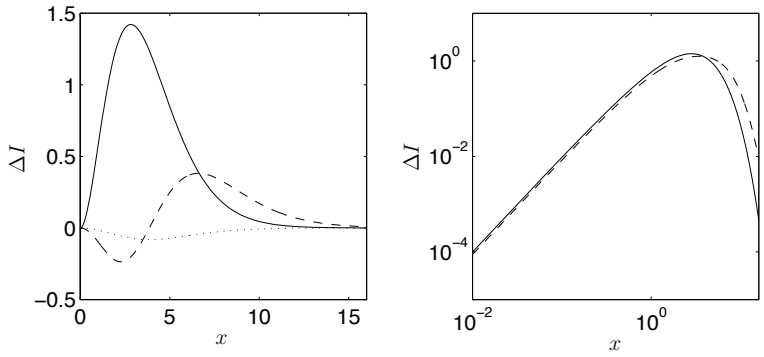

Figure 1: Blackbody spectrum of the CMB in units of $(hc)^2/(2(k_BT_0)^3)$ (solid lines), with the SZ spectrum shown for comparison. The dashed line in the left panel shows the thermal effect for $k_BT_e = 5$ keV, while the dotted line shows only the kinematic effect with $v_r = 500$ km/s (receding). The dashed line in the right panel shows the CMB spectrum with the thermal effect added. The SZ signals have been computed with $\tau = 0.01$ and multiplied with a factor 1000 for clarity.

2.2 The Relativistic Thermal Equation

Because of the low optical depth to Compton scattering typical for galaxy clusters, $\tau_T \sim 10^{-2}$, most photons are not scattered even once, rendering a diffusion approximation inadequate. Equation (2.1) is also manifestly non-relativistic, making it of little use at high electron temperatures (more than a few keV). Relativistic corrections were first calculated by Fabbri (1981); here we will follow the approach of Rephaeli (1995). Calculating the full re-distribution in phase space and taking into account the low scattering probability, one arrives at the following formula for the thermal intensity change (following the notation of Rephaeli and Yankovich 1997):

$$\Delta I(x,\eta) = I_0(x)\frac{x^3}{(e^x-1)}\tau_T[\Phi(x,\eta)-1]. \tag{2.5}$$

Here, $\eta \equiv m_ec^2/k_BT_e$, and $I_0(x)$ is the incident blackbody spectrum of the CMB. The function $\Phi(x,\eta)$ is defined in appendix C. Equation (2.5) is based on the assumption that the electrons follow a relativistic Maxwellian distribution, and derived accounting for a variable number of scatterings per photon.

The thermal effect vanishes at around $x = 3.83$ or $\nu = 217$ GHz, the latter assuming the standard scaling of the CMB temperature with redshift. This so-called crossover frequency, which we will denote x_0, is independent of electron temperature in the diffusion approximation, but increases slightly with T_e when equation (2.5) is applied. Although the kinematic effect is slight, the peculiar velocity has a stronger influence on x_0, owing to the fact that the peak of ΔI_k (the latter having the same shape as the CMB blackbody) occurs at approximately the crossover frequency of the purely thermal

effect. The location of the crossover frequency can be approximated by (Sazonov & Sunyaev 1998b)

$$x_0 = 3.83\left(1 + 0.3\frac{v_r}{c}\frac{m_e c^2}{k_B T_e} + 1.1\frac{k_B T_e}{m_e c^2} + 1.5\frac{v_r}{c}\right), \tag{2.6}$$

with our convention of a positive v_r for a receding cluster. Equation (2.6) is a fit to results from a Monte Carlo simulation of the combined effects of v_r and T_e (Sazonov & Sunyaev 1998a). The "interference term" proportional to $v_r/(k_B T_e)$ shows a first-order coupling of the thermal and kinetic effects.

Figure 2 shows the shape of the intensity shift due to the thermal effect ($v_r = 0$) at

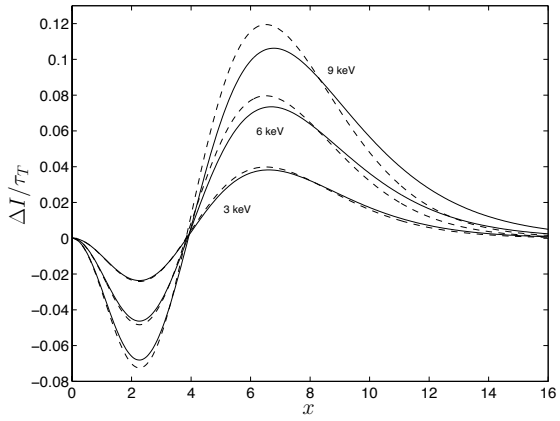

Figure 2: Spectral shape of the intensity change ΔI due to the thermal SZ effect. Solid lines show $\Delta I/\tau_T$ in units of $(hc)^2/(2(k_B T_0)^3)$, computed from equation (2.5) at $k_B T_e = 3$, 6 and 9 keV. Dashed lines show corresponding intensity shifts computed from the non-relativistic diffusion approximation (equation 2.1).

different electron temperatures. The difference between the diffusion approximation and the relativistic treatment is obvious already at 6 keV. The effect of equation (2.3) is shown in figure 3, where the frequency bands of the Planck high-frequency intrument are indicated (see section 3.3). The total SZ effect is also shown for a range of typical peculiar velocities, making the shift of x_0 due to the kinematic effect evident. Note how the whole spectrum is shifted toward lower wavelengths and intensities as v_r increases, while the effect of T_e mostly lies in shifting the amplitude of the spectrum, affecting the shape only slightly (not at all in the non-relativistic case). The latter implies that ratios of $\Delta I(\nu)$ at different frequencies ν_1 and ν_2,

$$r_F(\nu_1, \nu_2, T_e, v_r) \equiv \frac{\Delta I_1(\nu_1, T_e, v_r, \tau_T)}{\Delta I_2(\nu_2, T_e, v_r, \tau_T)}, \tag{2.7}$$

will exhibit a weak dependence on the electron temperature, a fact which we will take advantage of when fitting to a temperature-redshift relation. Note also that r_F is

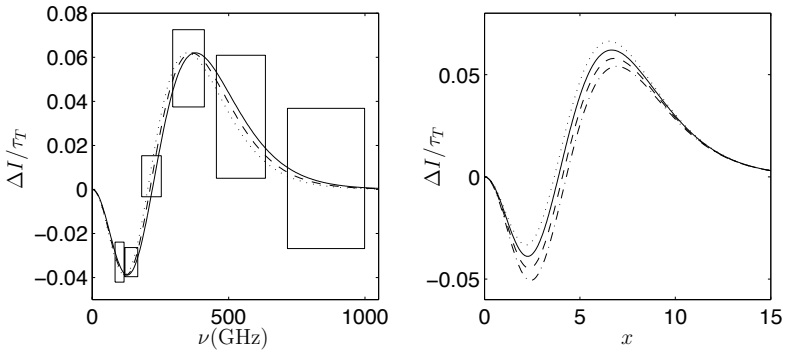

Figure 3: Shape of the SZ spectrum ΔI at $k_B T_e = 5$ keV. The left panel shows the effect of varying the parameter a: the solid line has been computed for $a = 0$, while the dashed and dotted represent $a = 0.1$ and $a = 0.2$, respectively. The frequency bands of the Planck satellite are indicated, with vertical sizes representing relative noise levels. The right panel shows the SZ spectrum for different v_r. Solid line: $v_r = 0$. Dotted line: $v_r = -500$ km/s (approaching). Dashed and dash-dotted lines: $v_r = 500$ km/s and $v_r = 1000$ km/s, respectively (receding). Units of intensity are those of figure 2.

independent of the optical depth τ_T, which is readily seen from equations (2.1) and (2.5).

The redshift dependence drops out from r_F when the standard $T - z$ relation is applied, but there is a pronounced z dependence in the general case, as illustrated in figure 4 for a pair of frequencies well below the crossover frequency. The magnitude of the dependence varies with ν_1 and ν_2, as well as with T_e and v_r. The choice of frequencies is also important for other reasons, which will be elaborated upon in section 4.

3 Simulating the Large-Scale Universe

Modeling the large-scale structure of the universe and the clustering of the cold dark matter does not only require precise knowledge of the current values of the cosmological parameters, such as σ_8, Ω_M and h, but also relies heavily on the standard Friedman-Robertson-Lemaitre-Walker (FLRW) cosmology as the clustering of matter is highly sensitive to the z dependence of the cosmological parameters (appendix D).

In observational astronomy, however, much of the dependence is shifted to the sensitivity of the instrumentation used in observations; as we go to high redshifts ($z \sim 1$) we will only be able to detect the most massive dark matter halos. Thus, there is a redshift-dependent limiting mass $M_{\rm lim}$, depending heavily on the instrumentation in question, which will limit our simulated observations. Given the sensitivity of the Planck high frequency instrument, we can compute $M_{\rm lim}$ for our fiducial cosmology

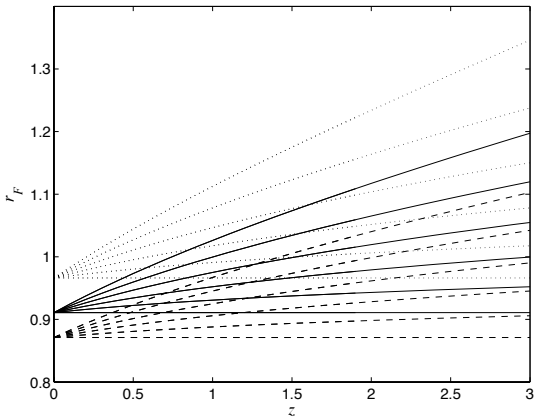

Figure 4: Theoretical r_F as a function of redshift for the SZ intensity distortion at $\nu_1 = 100$ GHz and $\nu_2 = 143$ at $k_B T_e$ =3, 6 and 9 keV (dashed, solid and dotted lines). Relativistic case with $v_r = 0$. The dimensionless parameter a varies from 0 to 0.1 from bottom to top for each temperature.

and obtain a catalog of observable clusters. Below this mass we need not be concerned with the structure of mass inhomogeneities.

3.1 The Mass Function

The Press-Schechter formalism (Press & Schechter 1974) estimates the comoving number density of clusters in a given range of mass and redshift based on the two-point correlation function of mass inhomogeneities and assuming spherical in-fall for the collapse of over-dense regions.

A slightly modified variant based on ellipsoidal in-fall, suggested by Sheth & Tormen (1999), has been found to correspond well with N-body simulations. In particular, the model agrees well with simulations due to Jenkins et al. (2001), although the formula of Sheth & Tormen gives a slightly higher number of clusters at the high-mass end. The number of clusters per unit of comoving volume at redshift z and with mass in the interval $(M,\ M + \mathrm{d}M)$ is given by

$$n(M, z)\mathrm{d}M = A\left(1 + \frac{1}{\nu'^{2q}}\right)\sqrt{\frac{2}{\pi}}\frac{\bar{\rho}_0}{M}\frac{\mathrm{d}\nu'}{\mathrm{d}M}e^{-\frac{\nu'^2}{2}}\mathrm{d}M, \tag{3.1}$$

where the various constants and functions are explained in detail in appendix E. Although the z dependence in σ_8 is currently well understood, $n\,\mathrm{d}M$ is particularly sensitive to the choice of $\sigma_8(z = 0)$, a parameter which is not yet constrained to a high accuracy. A description of the systematic error due to the choice of the current value of σ_8 is described by Wang & Steinhardt (1998).

The rapid decrease in number counts with increasing mass is illustrated in figure 5, which shows $n(M)$ at different redshifts.

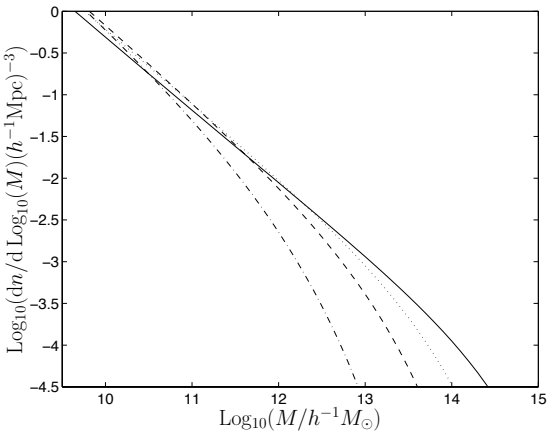

Figure 5: The mass function (equation 3.1) per decade of mass for our fiducial cosmology at different redshifts: $z = 0$ (solid line), $z = 1$ (dotted line), $z = 2$ (dashed line) and $z = 4$ (dash-dotted line). Adapted from Reed et al. (2003).

Multiplying (3.1) with the comoving volume element

$$V(z) = \frac{D_A(z)^2(1+z)^2}{H(z)},$$

where D_A is the angular diameter distance (appendix D.4) and H is the dimensionful Hubble parameter (appendix D.1), and integrating over mass, one obtains the distribution of observable clusters with respect to redshift as

$$\frac{dN}{dz} = c\int^{\infty} V(z)n(M,z)\mathrm{d}M, \tag{3.2}$$

where c is the speed of light in vacuum. The integration is taken from the minimum mass required for detection of a dark matter halo at redshift z, $M_{\mathrm{lim}}(z)$, which is related to the limiting observable flux S_{lim} of the instrumentation.

3.2 Cluster Detection

Holder et al. (2000) have determined M_{lim} for an interferometric array of ten 2.5 m dishes at 30 GHz by performing mock observations on simulated SZE clusters. A more analytical account, which we will use here, is given by Fan & Chiueh (2001) (a similar formula is given by Battye & Weller 2003), in which the flux sensitivity S_ν at frequency

ν is related to mass M as

$$S_\nu = 2.29 \times 10^4 f(x) \times 1.70 \times 10^{-2} h \left(\frac{f_{\rm ICM}}{0.1}\right) \times \left(\frac{1+X}{1.76}\right) \left(\frac{7.75}{0.5\,|{\rm d}\ln\rho_{\rm gas}(r)/{\rm d}\ln r|_{r_{\rm vir}}}\right) \times \left(\frac{6.8}{5X+3}\right) \left(\frac{D_A}{100\,h^{-1}\,{\rm Mpc}}\right)^{-2} (1+z) \times \left(\frac{\Omega_M(0)}{\Omega_M(z)}\right)^{1/3} \left(\frac{\Delta_c}{178}\right)^{1/3} \left(\frac{M}{10^{15}\,h^{-1}M_\odot}\right)^{5/3} {\rm mJy}, \tag{3.3}$$

where $f(x)$ is the spectral shape factor introduced in section 2, $f_{\rm ICM}$ is the ICM gas fraction, X is the hydrogen mass fraction and D_A is the angular diameter distance. Δ_c is the over-density of the cluster at the redshift $z_{\rm vir}$ of virialization, given for our ΛCDM model in appendix D.3. We will assume $z_{\rm vir} = z$ for the remainder of this paper. Only the thermal SZ effect is considered in the derivation of (3.3).

The factor $|{\rm d}\ln\rho_{\rm gas}(r)/{\rm d}\ln r|_{r_{\rm vir}}$, equal to 2 in the case of the isothermal sphere (e.g. Kitayama & Suto 1996), should be calculated using the proper density profile. In this paper we use the approach outlined in Tang & Fan (2003), with the gas density profile of Navarro, Frenk & White (1997):

$$\left.\frac{{\rm d}\,\ln\rho_{\rm gas}}{{\rm d}\,\ln r}\right|_{r_{\rm vir}} = -\frac{1+3c}{1+c}, \tag{3.4}$$

where

$$c = 6\left(\frac{M_{\rm vir}}{10^{14}h^{-1}M_\odot}\right)^{-1/5}.$$

It is easily verified that taking $c = 5$ introduces an error smaller than 10 % in equation (3.4) for all masses relevant to our discussion.

Equation (3.3) can now be solved for $M_{\rm lim}$ given the limiting flux $S_{\rm lim}(\nu)$ at a given significance level. It should be pointed out that (3.3) is valid only for unresolved clusters; the case of a resolved cluster count is treated by Tang & Fan (2003). For reasons given below, it will be sufficient to regard the unresolved case for the purposes of this paper.

Already, we have to make assumptions about $T(z)$ when computing $f(x)$ from the dimensional observation frequency. The basic premise is that we assume the standard relation for the large-scale model of the universe outlined in this section, then we make small deviations from it when simulating observations to check for consistency.

3.3 The Cluster Catalog

Based on equation 3.3, we compute $M_{\rm lim}(z)$ for the frequencies of the Planck high frequency instrument. One sigma detection levels from Lamarre et al. (2003) are given in table 1 as flux sensitivities (S_ν). Only the lower frequencies will be of use

Table 1: Expected properties of the Planck high frequency instrument (Lamarre et al. 2003).

Central Frequency (ν)	GHz	100	143	217	353	545	857
Bandwidth	GHz	33	47	72	116	180	283
Angular Resolution	arcmin	9.2	7.1	5.0	5.0	5.0	5.0
Total Flux Sensitivity per pixel	mJy	14.0	10.2	14.3	27	43	49
Flux Sensitivity	Jy/sr	680	890	2500	4730	7530	8580

here, as the 545 GHz and 857 GHz channels will be largely obscured by dust emission. The frequency band centered at 217 GHz is not suited for calculating ratios, as it is too close to the crossover frequency.

To ensure detection, we use 3 sigma detection levels, computing $M_{\rm lim}$ for all the central frequencies and using the frequency with the highest limiting mass in a given redshift range when applying equation (3.2). Figure 6 shows S_ν for some of the relevant frequencies, assuming $a = 0$. As the different curves do not intersect, we simply use $\nu = 353$ GHz to compute $M_{\rm lim}$ across all redshifts, ensuring detection in all bands with lower limiting mass. Equation 3.2 is then applied, yielding a measure of the differential count of clusters of all observable masses with respect to z and per unit angular size on the sky. Integrating over z to infinity, we will have the total number of observable clusters per angular area element, allowing for a full-sky cluster count.

Differential cluster counts in the three frequency bands considered are shown in the right panel of figure 6. As expected, the 353 GHz band yields the lowest number of

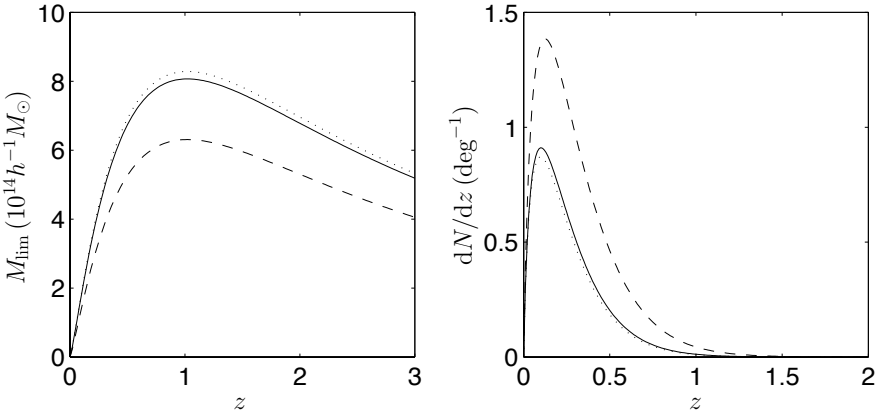

Figure 6: Limiting mass (left) and differential cluster counts (right) as functions of redshift in different frequency bands: $\nu = 100$ GHz (solid lines), $\nu = 143$ GHz (dashed lines) and $\nu = 353$ GHz (dotted lines).

clusters per square degree on the sky, yielding the total number of clusters, $N \sim 6000$, in a full-sky survey.

Taking a different from zero will generally shift $M_{\rm lim}$ downward as long as a is small and positive (as we have assumed), making the above a sufficient constraint on the number of observable clusters.

To simulate a cluster catalog, the normalized form of equation (3.2) is used as the probability density function for z in a random generation. Equation (3.1) should then be normalized for the redshift of each individual cluster to assign a mass using the same approach; due to the many consecutive integrations demanding extensive computing time, however, we make use of binning with z increments of 0.01.

For the purpose of simulating signals for mock SZE measurements we need to know the electron temperatures rather than the masses of the clusters. The normalization of the standard relation $T_e \sim M^{2/3}$ depends on how the density profile is taken. We use the relation

$$k_B T_e = \left(\frac{7.75}{0.5\,|\mathrm{d}\ln\rho_{\rm gas}(r)/\mathrm{d}\ln r|_{r_{\rm vir}}} \right) \left(\frac{6.8}{5X+3} \right) \times \left(\frac{M}{10^{15}\,h^{-1}M_\odot} \right)^{5/3} (1+z) \left(\frac{\Omega_M(0)}{\Omega_M(z)} \right)^{1/3} \left(\frac{\Delta_c}{178} \right)^{1/3} \mathrm{keV} \tag{3.5}$$

with the Navarro-Frenk-White density profile discussed above. Equation (3.5) is roughly consistent with recent observations (e.g. Finoguenov et al. 2001, Allen et al. 2001), although there is a large error margin from the rescaling to virial mass. We add a scatter to the temperature distribution by computing a standard deviation of 30 % of the values obtained from (3.5), then using a normal distribution to re-calculate each temperature. It should be mentioned that the previously introduced limiting mass relation of equation (3.3) also relies on (3.5).

To model peculiar velocities, we follow the approach of Sheth & Diaferio (2001), who suggest the formula

$$\sigma_{\rm halo}(M,z) = H_0 \Omega_0^{0.6} \sigma_{-1} \sqrt{1 - \frac{\sigma_0^4}{\sigma_1^2 \sigma_{-1}^2}}, \tag{3.6}$$

for the standard deviation of collective peculiar velocities of massive clusters as a function of mass and redshift. The indexed σ's in (3.6) are given by

$$\sigma_j^2(M) = \frac{1}{2\pi} \int_{k_{\rm min}}^{\infty} \mathrm{d}k\, k^{2+2j} P(k) W^2[kR(M)], \tag{3.7}$$

where the functions $P(k)$ and $W(x)$ are the same ones used for normalizing the power spectrum in the Sheth & Tormen mass function (see appendix E). The redshift dependence comes in through the cut-off mode $k_{\rm min}$ determined by the Hubble radius $L = c/H(z)$ within which there is causal contact between all regions of space. In our catalog, comprised mainly of clusters with low z, this dependence will be weak, allowing us to use the approximation

$$\sigma_{\rm halo}(M) = \frac{\sigma_{\rm fit}}{1 + (R/R_{\rm fit})^\eta}, \tag{3.8}$$

where for the fiducial model $\sigma_{\rm fit} = 414.7$ km s^{-1}, $R_{\rm fit} = 34.67\,h^{-1}$ Mpc, $\eta = 0.87$ and R is given by

$$R(M) = \left(\frac{3M}{4\pi\rho(z)}\right)^{1/3}, \tag{3.9}$$

where $\rho(z)$ is the mean density of the universe at redshift z.

For each cluster, we assign a velocity by taking a normal distribution with the standard deviation given by (3.8) and a mean of zero, dividing by a factor of $\sqrt{3}$ to get the radial part of the motion.

The distributions (data sets) of the relevant quantities of the simulation are illustrated in figure 7. Relevant correlations between the data sets are also shown.

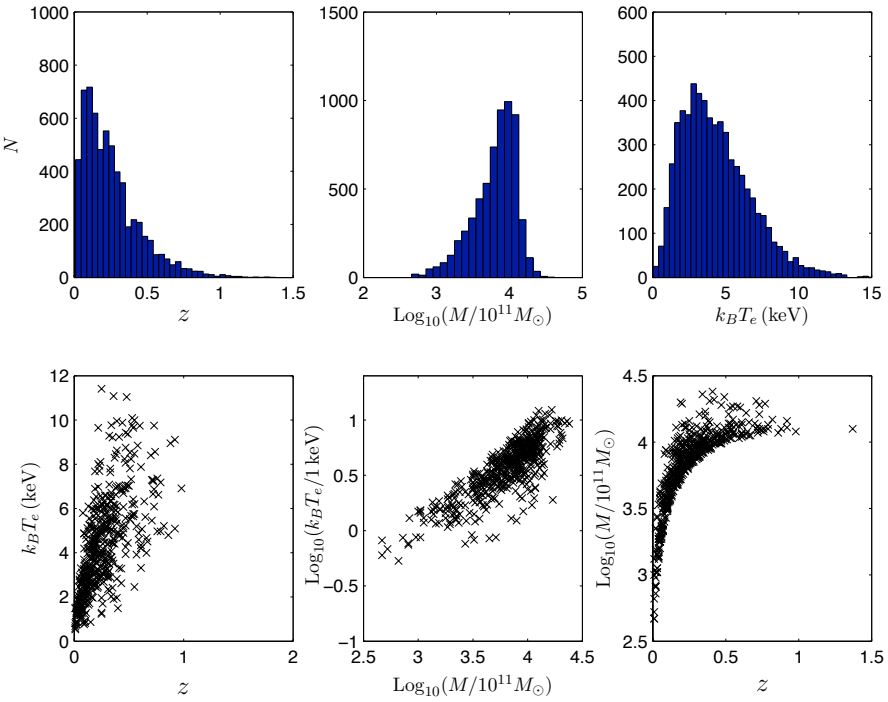

Figure 7: Histograms and correlations of the parameters in the cluster catalog. Upper left, middle and right: redshift distribution, mass distribution and temperature distribution, respectively. Lower left: The $z - T_e$ correlation. Lower middle: correlation of mass and temperature. Lower right: Scatter plot of mass versus redshift, clearly showing the behavior of the limiting mass. Scatter plots show only a sample of 500 clusters for clarity.

As already noted, the optical depth of a cluster needs not be known to take ratios from the SZ spectrum; however, we must model τ_T to get the strength of the SZ signal and ensuring the right error propagation. The Thomson optical depth is

$$\tau_T = \int n_e \sigma_T \mathrm{d}l, \tag{3.10}$$

where the integration is along the line of sight, n_e is the number density of electrons, and $\sigma_T = 6.65 \times 10^{-25}\,\mathrm{cm}^{-2}$ is the Thomson cross-section. From a simple spherical consideration, we will assume $\tau_T \sim M^{1/3}$, and normalize this relation using well-known clusters. For the Abell 2163 cluster, LaRoque et al. (2002) have found the Comptonization parameter $y = 3.56 \times 10^{-4}$, from which τ_T can be calculated (appendix B). For the same cluster, Markevitch et al. (1996) find the mass within 0.5 h^{-1} Mpc to be $4.3 \pm 0.5 \times 10^{14}\,h^{-1}\,M_\odot$. Interpreting this as the virial mass yields the relation

$$\tau_T = Q \left(\frac{M}{10^{11} M_\odot} \right)^{1/3} \tag{3.11}$$

where $Q = 8.01 \times 10^{-4}$ from the above data. As we have merely one data point, we will use half of this value as a worst-case scenario. With this approach, we will have an average τ_T of about 10^{-2} in the catalog.

4 Mock Observations

4.1 Conversion of Intensity to Flux

Mock observations of flux from our cataloged clusters are carried out by computing the SZ intensity shift at the frequencies specified in table 1, applying equations (2.4) and (2.5). We use the Planck bandwidths, initially assuming a top-hat frequency response of the filters. Observed SZ flux is simply the intensity change ΔI integrated over the angular size of the cluster, i.e.

$$S_\nu(x) = \int \Delta I_\nu(x)\,\mathrm{d}\Omega. \tag{4.1}$$

To carry out the integration over solid angle, we need to model the angular sizes of the clusters and convolve with the beam profile of a given frequency channel. As a first approximation to the angular size, we can compute the virial radius from the mass according to (e.g. Peebles 1980)

$$r_{\mathrm{vir}} = \left(\frac{M_{\mathrm{vir}}}{(4\pi/3)\rho_{\mathrm{crit}}(z)\Delta_c(z)} \right)^{1/3}, \tag{4.2}$$

and calculate the subtended angle θ on the sky as

$$\theta = 2\frac{r_{\mathrm{vir}}}{D_A}, \tag{4.3}$$

where $D_A(z)$ is the angular diameter distance. Applied to the cluster catalog, this approach will yield angular sizes on the order of, or greater than, the typical beam sizes of the Planck high frequency instrument (the latter ranging from 5 to 9.2 minutes of arc). However, such an approach does not account for beam convolution, and assuming a Gaussian profile for the beam, one finds that the majority of clusters are in fact unresolved (Kay et al. 2001).

Rather than modeling the flux with the full expressions taking into account the properties of the instrumentation, such as beam convolution and the sensitivities of the photometric channels, we will introduce an ad-hoc factor $t > 1$ of order unity with which the error can be amplified (this really amounts to the same as diminishing the signal since we will take ratios). We can then investigate how our fits to a and v_r will depend on t; in particular we will want the final fit to a to be as unbiased as possible regardless of the magnitude of the error. The introduction of the factor will also serve as to take into account any inaccuracy in the modeling of τ_T, as well as systematic errors not accounted for in the statistical error bars of Planck. In most of what follows, we will assume $t = 2$ unless otherwise stated.

Each flux is recorded adding a random (normally distributed) error using the standard deviations quoted in table 1 to the computed value, and simply multiplying by the factor t representing the remaining properties of the instrumentation.

4.2 Frequency Sensitivity of the Method

Finding a suitable frequency pair with which to fit to $T(z)$ amounts to little more than trial-and-error. We can, however, get a general idea of the sensitivity to the different parameters in the model by using arguments such as those of section 2.

Figures 8 and 9 illustrate the sensitivity of r_F to T_e and v_r at different frequency

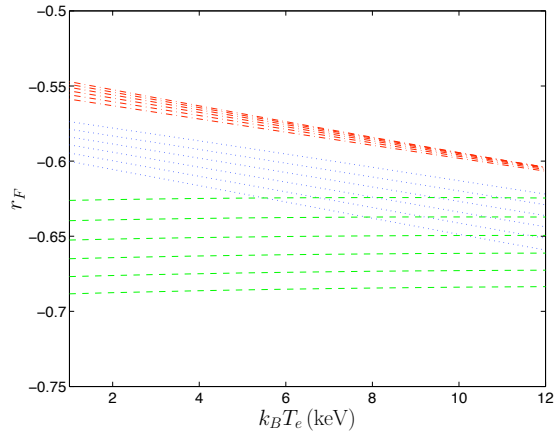

Figure 8: Flux ratio $r_F = S_1/S_2$ as a function of cluster temperature at $z = 0.5$ with a varying from 0 to 0.1 by 0.02 from bottom to top. The dashed lines represent the 100/143 GHz ratio, to which a constant -1.6 has been added for clarity, the dotted are the 143/353 GHz ratio, and the dash-dotted are the 100/353 ratio. Here, $v_r = 0$.

pairs. The a dependence which comes about for $z \neq 0$ is also seen. It is evident that those combinations sensitive to a are not necessarily also those most sensitive to the intrinsic cluster properties.

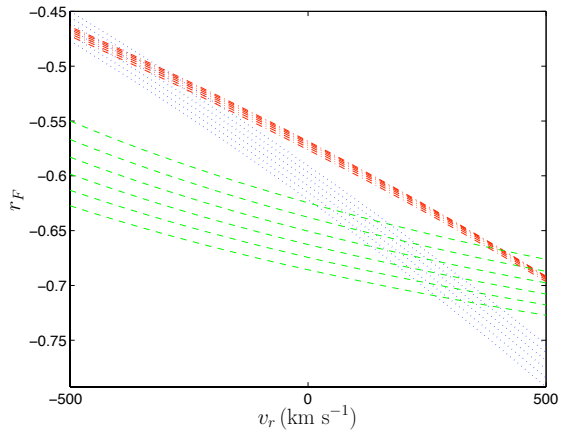

Figure 9: As for figure 8, but with $k_B T_e = 6$ keV and r_F varying with v_r. For clarity, a constant -1.6 has been added to the 100/143 GHz ratio.

It has already been mentioned that r_F is slightly more sensitive to v_r than to T_e for any useful frequency combination. This is unfortunate, as it is much easier to get T_e independently from follow-up (e.g. X-ray) observations. To obtain passable results, we will have to model peculiar velocities on a cluster-by-cluster basis. The most straightforward way of doing this is to find a separate flux ratio $r_F^{(v)}$ especially sensitive to v_r. As any such ratio will also be sensitive to even a small change in a, we will have to employ a method with which to fit to a and v_r simultaneously. This will be discussed in section 5.

5 Analysis

5.1 Error Propagation

For small errors, we can estimate the error in the ratio of flux S_1 and flux S_2 with standard error propagation as

$$\delta r_F = \frac{S_1}{S_2}\sqrt{\frac{\delta S_1}{S_1}^2 + \frac{\delta S_2}{S_2}^2}\,. \tag{5.1}$$

For errors larger than a few percent in S_1 and S_2, the error in r_F will exhibit a considerable skew due to the probability distribution of a ratio of normally distributed stochastic variables. To address this issue, we use the Boole-Bonferroni method, using the endpoints of a 68% confidence interval (1 sigma) for each flux to define a confidence interval for the ratio. The ratio confidence interval is then rescaled to 68% using the proper statistical factor, approximating with normal distributions on either side of the expectation value.

For simplicity, we assume precise and unbiased knowledge of the electron temperatures in the catalog, and account for errors in measurements of such by somewhat overestimating our remaining errors. We will have to model the errors due to peculiar velocities more carefully; not only because of the limited precision with which these can be fitted for from the SZ data, but also because r_F is more sensitive to v_r than to T_e.

We will use a separate frequency ratio $r_F^{(v)}$ with $\nu_1 = 143GHz$ and $\nu_2 = 353GHz$ when fitting to v_r for each individual cluster. Error bars on each peculiar velocity will be converted into error bars in the ratio r_F used for the CMB temperature by simply calculating this ratio at the endpoints of the 68% confidence interval of v_r. The systematic errors are then added in quadrature to the random errors.

5.2 Statistical Tests of the Data

To get an idea of how well we should expect to be able to constrain the $T-z$ relation, we initially conduct statistical tests of how well (hypothetical) universes of with different $T(z)$ can be distinguished when using the type of data described in the above.

Figure 10 gives a first indication of how the inclusion of v_r severely mixes distributions with different a, making clusters at high redshifts especially important. To get

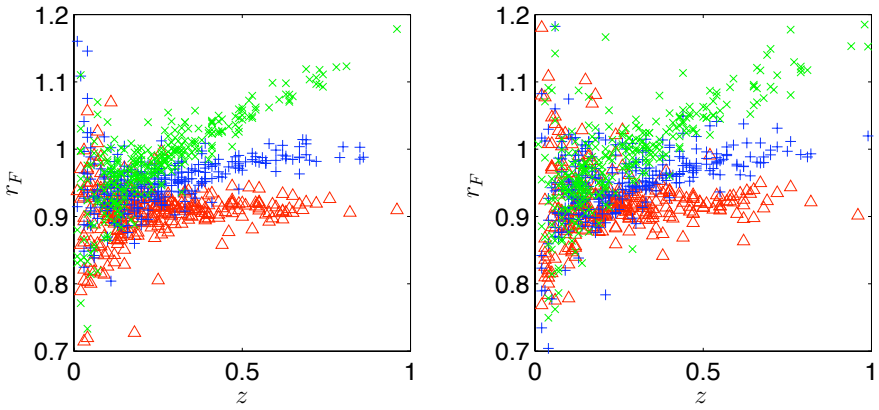

Figure 10: Comparison of data sets for the 100/143 GHz ratio acquired using $v_r = 0$ (left) and simulated peculiar velocities (right) for different T - z relations: $a = 0.0$ (triangles), $a = 0.1$ (crosses) and $a = 0.2$ (x-marks). Compare to figure 4.

a first quantitative measure, ratio distributions acquired using different values of a, a_i and a_j, are compared to see how small we can make $\Delta a \equiv |a_i - a_j|$ while still being able to distinguish the data sets (typically, $a_j = 0$ is used). The Kolmogorov-Smirnov (KS) statistical test is employed in testing whether the data sets are distinct; in particular, the significance level p for the null hypothesis that the data sets are drawn from the same statistical distribution is computed for each Δa. The influence of the size of the

cluster catalog in distinguishing the data sets is also investigated. For the time being, we adopt the somewhat arbitrary (and rather generous) convention of taking two data sets for which p is below the value 0.01 to be distinguishable. In the next section we will offer a more precise treatment of constraining a.

Figure 11 shows the results of our statistical tests for different sizes of cluster

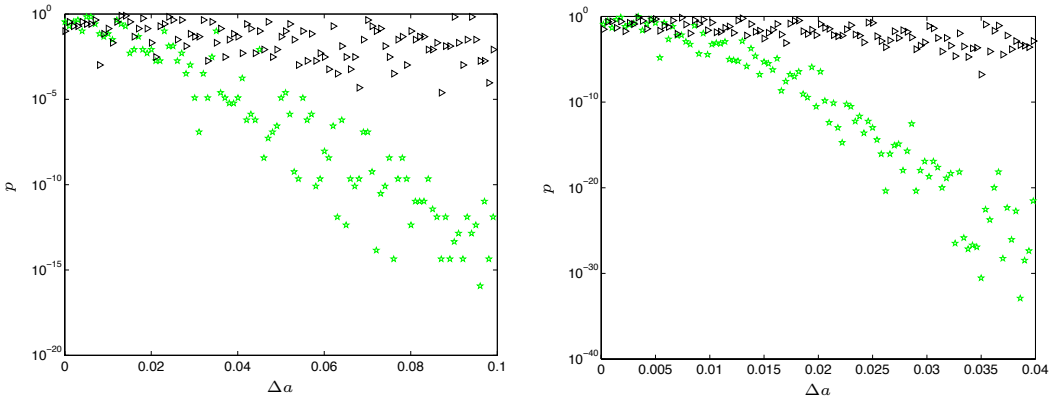

(a) 100 clusters for each value of a.

(b) 1000 clusters for each value of a.

Figure 11: Kolmogorov-Smirnov tests for mock observations of cluster catalogs of varying sizes and for varying a. Pentagrams show significance levels p (see text) for the 100/143 GHz ratio, while corresponding tests for the 143/353 GHz ratio are represented by triangles.

catalogs. Of our sample ratios, the 100/143 GHz ratio, henceforth r_{F12}, is clearly the most suitable for constraining the temperature redshift-relation. KS tests have been carried out for all the ratios appearing in figures 8 and 9; however, only the two with the most favorable results are shown in figure 11.

These initial tests are promising; using observations of as little as 100 clusters, we should be able to tell apart models which differ in a by as little as 0.02. The 100/143 GHz ratio is orders of magnitude more sensitive to a than the other ratios; it will therefore suffice to use this ratio in the subsequent analysis, and it will not be of any practical use to combine measurements at more than two frequencies. The sample size shown in figure 11(b) is close to the size of our simulated catalog; we should therefore expect the error in a fit to a to be on the order of the Δa distinguishable in the tests described here.

5.3 Fits to v_r and a

Owing to the degeneracy of v_r and a, it is not possible to fit to one without knowing the other. It is also difficult to carry out a fit for both parameters at the same time, since the former is a parameter unique for each cluster, and the latter is a universal

constant, valid for all clusters in the catalog. We therefore make use of the following iterative procedure to find a:

1. As a first guess, $a_{(i)} = a_{(0)} = 0$ is chosen.
2. Each cluster in the catalog is fitted to v_r using a χ^2-fit to the 143/353 GHz ratio (in most cases, this really amounts to nothing more than solving for v_r numerically, as we have only one data point). Errors are modeled according to section 5.1.
3. Using the velocities from step 2, $a_{(i+1)}$ is estimated from a χ^2-fit of the 100/143 GHz ratio to the entire catalog.
4. Step 2 is repeated with the new value of a obtained in step 3. Iteration is continued until self-consistency is achieved or until a diverges.

The criterion for divergence in step 4 is obvious; if it is the case that $|a_{(i+1)} - a_{(i)}| > |a_{(i)} - a_{(i-1)}|$ for a succession of iterations, the method is failing. It has been found, however, that separate occurrences of such inconsistencies can still lead to a subsequent convergence.

The convergence criterion is

$$|a_{(i+1)} - a_{(i)}| < \epsilon$$

for some sufficiently small ϵ chosen such that $\epsilon \ll \sigma_a$, where σ_a is the estimated error in a at the 68% confidence level:

$$\frac{1}{\sigma_a^2} = \frac{1}{2}\frac{\partial^2 \chi^2}{\partial a^2}. \tag{5.2}$$

Typically, the velocities inferred from step 1 have error bars roughly the same order of magnitude as the velocities themselves, making these results of little use other than for the following fit to a.

6 Results

In general, the iterative process described above converges in less than ten iterations for all $a < 0.2$. For our fiducial cosmology with a catalog of about 6000 clusters, we find $\sigma_a \simeq 5 \times 10^{-4}$ when setting $a = 0$, which means we should be able to constrain a to an accuracy of 10^{-3} at the 95% confidence level, assuming the statistical method is robust and without bias. Using other values of a in the relevant range has merely a weak impact on σ_a. To test the robustness of the method, several consecutive simulations have been run with $a = 0$ as input, and the results of the fits are shown in figure 12. Any deviation from $a = 0$ on average is orders of magnitude smaller than σ_a, and the skew of the distribution is negligible. Moreover, the value of σ_a estimated from equation (5.2) is in agreement with the spread of the consecutive fits. It is also

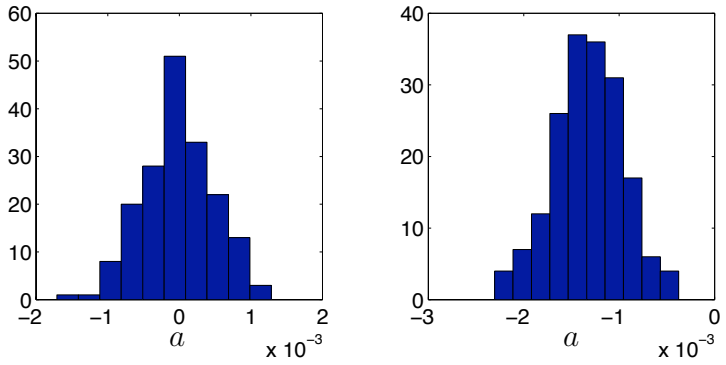

Figure 12: Histograms of fits to 180 consecutive simulations, all with $a = 0$ as input. The left panel shows the result when first fitting to v_r, and the right shows the resulting bias when $v_r = 0$ is assumed in the fit to a.

obvious from figure 12 that it is insufficient to fit to a assuming $v_r = 0$; although the expectancy value of the velocity distribution is zero, the non-linear contributions of velocities with opposing signs to r_F do not cancel.

A sample of fitted velocities from a final iteration is shown in figure 13. The

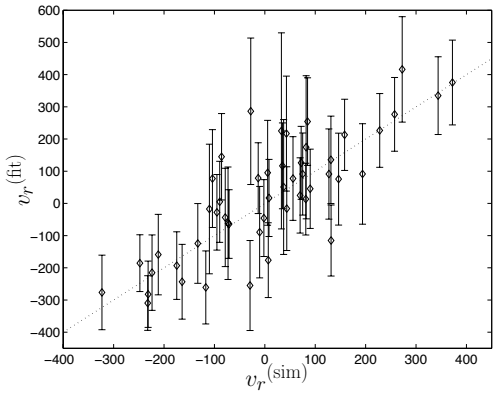

Figure 13: Sample of 50 fitted peculiar velocities ${v_r}^{(\mathrm{fit})}$ with error bars versus simulated velocities ${v_r}^{(\mathrm{fit})}$. The dotted line shows the desired ${v_r}^{(\mathrm{fit})} = {v_r}^{(\mathrm{sim})}$. $a = 0$ was used as input in the simulation.

distribution of peculiar velocities can also be used as a check that we are converging towards the correct value of a. We expect the distribution to approach not the original one, but one with additional scatter from the uncertainty in the fit. The mean should approach zero, and the skew should be small. This is illustrated in figure 14.

Next, we study the effects of varying the cluster catalog size N and the magnitude of the error in recorded flux, the latter described in terms of the parameter t discussed

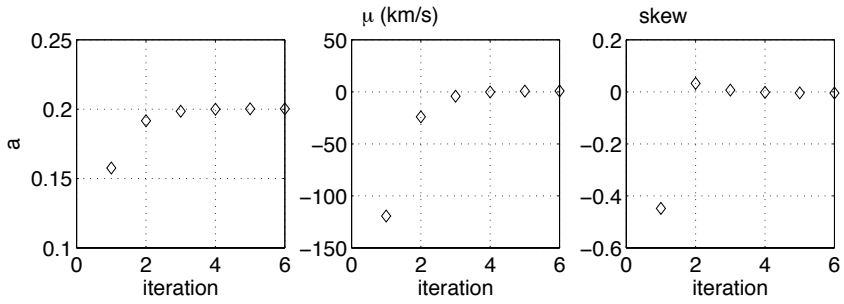

Figure 14: Convergence of the method, verified by estimated moments of the velocity distribution. As a approaches the value 0.2 used in this particular simulation, the mean and skew of the v_r distribution approach zero.

in section 4.1. $t = 2$, which has been used in the above, corresponds to an average error of about 12 % in individual flux recordings for all relevant frequency bands. The influence of N and t on σ_a is shown in figure 15 for a set of simulations. Assuming

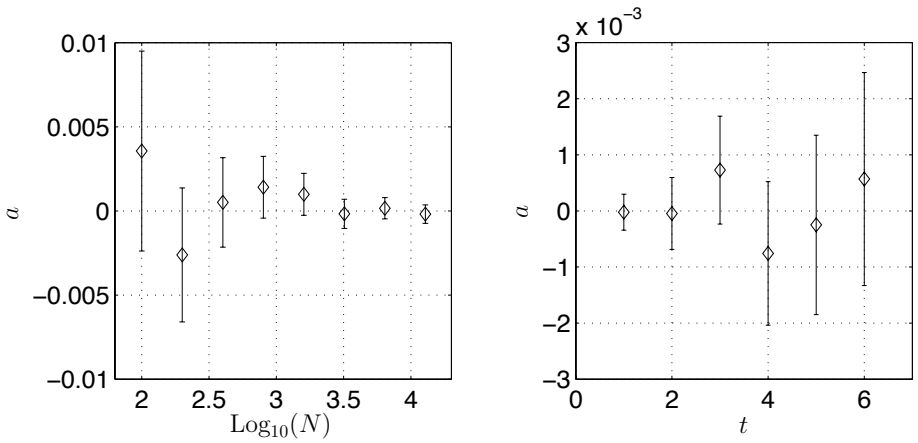

Figure 15: 68 % confidence intervals on a from simulations varying in catalog size N (left) and in the parameter t (right). $t = 2$ in the left panel, while $N = 6000$ has been used when varying t.

$t = 2$, the results indicate that a sample of as little as 100 clusters can constrain a to a precision of about 0.01. In the range of t studied (up to an average error of about 40 % in flux), no bias with respect to a has been found.

7 Conclusion

We have investigated the possibility to constrain the cosmological temperature-redshift relation using ratios of SZ observations in different frequency bands. We have seen that this approach to some extent diminishes the effects from parameters unique for each cluster, although these parameters must be modeled for an accurate treatment. A simulation of observations on about 6000 galaxy clusters has been employed to test the method. The basic assumptions are the following:

1. The temperature-redshift law is parameterized as $T = T_0(1 + z)^{(1-a)}$, where $0 \leq a < 0.2$ from theory and previous observations.

2. We choose a fiducial ΛCDM cosmology with (Ω_M, Ω_Λ, h, σ_8) = (0.3, 0.7, 0.7, 0.9) and assume a full-sky survey.

3. The Sheth-Tormen mass function for the distribution of dark matter halos in the universe is assumed.

4. The electron temperature and redshift of each cluster are assumed to be known.

The fiducial cosmology chosen has no impact on the method devised for fitting to the parameter a from a catalog of clusters. It does, however, have a strong influence on the distribution of observable clusters at different redshifts, and influences the precision with which the T-z relation can be constrained.

After initial tests, we have chosen the 100/143 GHz frequency pair for the fit to a, while the 143/353 GHz pair has been found useful when fitting to v_r. The main results can be summarized as follows:

1. The parameter a can be constrained to within 10^{-3} at the 95 % confidence level from a catalog of about 6000 cluster inferred from the fiducial cosmology and assuming the resolution of the Planck high-frequency instrument.

2. The iterative process of fitting to a and v_r is found to converge without bias for $a \leq 0.2$ and with average errors in flux up to at least 40%.

3. Fitting to a without first fitting to v_r introduces a bias with respect to a with an offset of about 2×10^{-3} as a result. Thus, for a catalog of clusters significantly smaller than our simulated one, it would be sufficient to assume $v_r = 0$ in a fit to a, as the error in a would be much greater than the bias.

Electron temperatures could be inferred from X-ray observations, but this would require lengthy follow-up observations. Furthermore, X-ray observations give electron temperatures in the centers of galaxy clusters, and such temperatures could vary significantly from the effective line-of-sight values responsible for thermal SZ spectra. Developing our method further, it would be possible to fit to T_e from data in an appropriately chosen pair of frequency bands. Such an approach would simply introduce

an additional step in the iterative method described in the above, but would also contribute to larger errors in the fit to the T-z relation with a possible bias as a result. This is a problem which will need to be investigated further.

It remains to model the systematic errors in the data introduced by contamination from astrophysical sources which emit in the relevant SZ frequencies. Recent findings suggest that interstellar dust emission, infra-red galaxies and primary CMB anisotropies can be responsible for systematic errors up to a factor of 5 times larger than the expected error bars for the Planck high-frequency instrument (Aghanim et al. 2004). This could put severe limitations on the estimation of any cosmological or cluster parameter from blind SZ surveys.

A The Temperature of the CMB in the Standard (FLRW) Cosmology

In the standard hot Big Bang model, the early universe is an almost perfect blackbody, photons being continuously created, absorbed, annihilated and re-emitted. Under such conditions, we expect the mean number of photons in a given oscillation mode to follow a Planck distribution characterized by a single temperature T:

$$\bar{n} = \frac{1}{e^{h\nu/k_B T} - 1}, \tag{A1}$$

where ν is the frequency of the oscillation mode with wavelength $\lambda = c/\nu$.

At a given cosmic epoch, we divide all of space into identical boxes with volume $V = L^3$, where $L \gg \lambda$ and $\lambda = 2\pi/k$ (where k is the wavenumber) is the longest wavelength under consideration. For the plain wave of each oscillation mode, $\psi = e^{i\mathbf{k}\cdot\mathbf{r}}$, we impose periodic boundary conditions of the form

$$\begin{aligned} \psi(x + L, y, z) &= \psi(x, y, z), \\ \psi(x, y + L, z) &= \psi(x, y, z), \\ \psi(x, y, z + L) &= \psi(x, y, z). \end{aligned} \tag{A2}$$

This will quantize the propagation vector $\mathbf{k}$, which we write

$$\mathbf{k} = \frac{2\pi\mathbf{n}}{L}, \tag{A3}$$

with $\mathbf{n} = (n_x, n_y, n_z)$ a set of integers. It is now straightforward to calculate the number of possible plane wave states between $\mathbf{k}$ and $\mathbf{k} + \mathrm{d}\mathbf{k}$. One finds

$$\Delta N_k = \frac{V}{(2\pi)^3} 4\pi k^2 \mathrm{d}k, \tag{A4}$$

where the factor 4π comes from an integration over all possible emission angles. Taking into account that there are two possible polarization states for each photon with frequency ν, we can compute the number density of photons per unit volume with frequency between ν and $\nu + \mathrm{d}\nu$. From (A1) and (A4) we find

$$n(\nu; T)\mathrm{d}\nu = \frac{4}{c^3} \frac{\nu^2 \mathrm{d}\nu}{e^{h\nu/k_B T} - 1}. \tag{A5}$$

To relate these results to the temperature of the microwave background today, consider the definition of the redshift,

$$1 + z \equiv \frac{\lambda_{\mathrm{obs}}}{\lambda_{\mathrm{emit}}}, \tag{A6}$$

implying that

$$\nu_0 = \frac{\nu}{1 + z}. \tag{A7}$$

Equation (A7) allows us to re-scale (A5) to the present:

$$n(\nu;T)\mathrm{d}\nu = n(\nu;T_0)\mathrm{d}\nu_0 \cdot (1+z)^3, \tag{A8}$$

i.e. the photon density preserves the blackbody spectrum and scales as the inverse volume of the universe. The temperature then decreases linearly with the radial scale, which in the FLRW model is simply $(1+z)$:

$$T_0 = \frac{T(z)}{1+z},$$

or, equivalently,

$$T = T_0(1+z). \tag{A9}$$

B A Non-Relativistic Derivation of the Thermal SZ Effect

In a non-relativistic scattering process, the change in the occupation number $n(\nu)$, where ν is the frequency, is approximated by the Kompaneets equation

$$\frac{\partial n}{\partial y} = \frac{1}{x_e^2}\frac{\partial}{\partial x_e} x_e^4 \left(\frac{\partial n}{\partial x_e} + n + n^2 \right), \tag{B1}$$

where $x_e \equiv h\nu/k_B T_e$ and T_e is the electron temperature characteristic for the scattering (do not confuse x_e with $x \equiv h\nu/k_B T_0$). The change of $n(\nu)$ is given with respect to the Comptonization parameter y, which in the case of radiation passing through an electron cloud can be written

$$y = \int n_e \sigma_T \frac{k_B T_e}{m_e c^2} \mathrm{d}l, \tag{B2}$$

where n_e is the number density of the electron gas. σ_T is the Thomson cross-section, and $(n_e\sigma_T)^{-1}$ can thus be interpreted as the scattering mean free path. The integration is along the line of sight of the electron cloud. Since the CMB is significantly colder than an electron cloud in a galaxy cluster, x_e is sufficiently small to rewrite the Kompaneets equation as

$$\frac{\partial n}{\partial y} = \frac{1}{x_e^2}\frac{\partial}{\partial x_e} x_e^4 \frac{\partial n}{\partial x_e}.$$

The right hand side of this equation is homogeneous, which allows us to replace x_e by x. Then, changing variables from x, y to ξ, y, the substitution $\xi = 3y + \ln x$ yields

$$\frac{\partial n}{\partial y} = \frac{\partial^2 n}{\partial \xi^2},$$

and the solution to this equation can be written in the form

$$I(\nu) = \int_{-\infty}^{\infty} \frac{1}{\sqrt{4\pi y}} \exp\left(-\frac{(s+3y)^2}{4y} \right) I_0(\nu_0)\mathrm{d}s, \tag{B3}$$

where $s = ln(\nu/\nu_0)$ and it is assumed that scattering occurs from frequency ν_0 to ν. $I_0(\nu)$ is the intensity of the incident CMB blackbody spectrum, i.e.

$$I_0(\nu) = \frac{2h\nu^3}{c^2}\left(e^{h\nu/k_BT_0} - 1\right)^{-1}. \tag{B4}$$

At low optical depth and low temperatures, y is sufficiently small to render the approximation

$$\frac{\partial n}{\partial y} = \frac{\Delta n}{y}$$

valid. This may be used directly in the simplified Kompaneets equation to obtain

$$\Delta n = xy\frac{e^x}{(e^x-1)^2}(x\coth(x/2) - 4), \tag{B5}$$

with a corresponding intensity shift given by

$$\Delta I(x) = x^3\Delta n(x) i_0, \tag{B6}$$

where $i_0 = 2(k_BT_0)^3/(h^2c^2)$. This result can also be obtained directly from taking (B3) in the limit of small y.

It is convenient to introduce the *spectral shape factor*

$$f(x) \equiv \frac{x^4e^x}{(e^x-1)^2}\left(x\coth(x/2) - 4\right) = \frac{x^4e^x}{(e^x-1)^2}\left(x\frac{e^x+1}{e^x-1} - 4\right) \tag{B7}$$

to take care of the x dependence in $\Delta I(x)$. Furthermore, the Comptonization parameter y is often expressed in terms of the Thomson optical depth τ_T. The relationship is

$$\tau_T = \int n_e\sigma_T \mathrm{d}l = y\frac{m_ec^2}{k_BT_e},$$

where once again the integration is along the line of sight. It is usually assumed that T_e is constant throughout a galaxy cluster, and so it is not included in the integration.

Expressed in terms of τ_T and $f(x)$, the intensity shift from the thermal SZE is

$$\Delta I(x) = \frac{2(k_BT_0)^3}{h^2c^2}\frac{k_BT_e}{m_ec^2}f(x)\tau_T, \tag{B8}$$

which is our final expression.

C Relativistic SZ Formulae

The following expressions, taking into account relativistic effects on the thermal SZ effect, are derived using a frequency redistribution based on a fully relativistic velocity distribution, derived by Rephaeli (1995). The latter article contains a number of typographical errors, and the expressions given here are those of Rephaeli and Yankovitch (1997). The spectral distortion is given by

$$\Delta I(x,\eta) = \tilde{I}_0(x)\tau_T[\Phi(x,\eta) - 1], \tag{C1}$$

where $\eta = m_e c^2/k_B T_e$ and $\tilde{I}_0(x) = I_0(x)x^3/(e^x - 1)$. As usual, $I_0(x)$ is the incident blackbody spectrum. Furthermore,

$$\Phi(x, \eta) = A(\eta)[\phi_1(x, \eta) + \phi_2(x, \eta)], \tag{C2}$$

where

$$\phi_1(x, \eta) = \int_0^1 \frac{t(e^x - 1)dt}{e^{xt} - 1} \int_{\beta_m}^1 \beta\gamma e^{-\eta(\gamma-1)} d\beta \int_{\mu_m}^1 q_1(t, \mu, \beta) \mathrm{d}\mu, \tag{C3}$$

$$\phi_2(x, \eta) = \int_0^1 \frac{(e^x - 1)dt}{t^3(e^{x/t} - 1)} \int_{\beta_m}^1 \beta\gamma e^{-\eta(\gamma-1)} d\beta \int_{-1}^{\mu_M} q_2(t, \mu, \beta) \mathrm{d}\mu. \tag{C4}$$

In these expressions, γ is the Lorenz factor at velocity $v = \beta c$, $\beta_m = (1-t)/(1+t)$, $\mu_m = (1 - t - t\beta)/\beta$, and $\mu_M = (t - 1 + \beta)/\beta$. The functions q_1 and q_2 are given by

$$q_1(t, \mu, \beta) = \frac{(3\mu^2 - 1)[(1 - \beta\mu)/t - 1]^2/\beta^2 + 3 - \mu^2}{(1 - \beta\mu)^2}; \tag{C5}$$

$$q_2(t, \mu, \beta) = \frac{(3\mu^2 - 1)[(1 - \beta\mu)t - 1]^2/\beta^2 + 3 - \mu^2}{(1 - \beta\mu)^2}, \tag{C6}$$

while $A(\eta)$ is defined as

$$A(\eta) = \frac{3}{32 \int_0^1 \beta^5 \gamma^2 e^{-\eta(\gamma-1)} \mathrm{d}\beta}. \tag{C7}$$

Note that γ is easily expressed in terms of β:

$$\gamma = \frac{1}{\sqrt{1 - \beta^2}}.$$

D The Redshift Dependence in Some Cosmological Parameters and Quantities

D.1 The Hubble Constant

Ignoring the effects of radiation, the z dependence in the expansion rate of the universe is given by

$$H^2(z) = H_0^2[\Omega_M(1 + z)^3 + (1 - \Omega_M - \Omega_\Lambda)(1 + z)^2 + \Omega_\Lambda], \tag{D1}$$

where H_0 is the value of the Hubble constant at the present epoch, and Ω_M and Ω_Λ are the matter density and dark energy density, respectively, at $z = 0$ and in units of the critical density

$$\rho_{\mathrm{crit}} = \frac{3H_0^2}{8\pi G}.$$

For brevity, we define the quantity

$$E^2(z) \equiv \left(\frac{H(z)}{H_0}\right)^2 = \Omega_M(1 + z)^3 + (1 - \Omega_M - \Omega_\Lambda)(1 + z)^2 + \Omega_\Lambda. \tag{D2}$$

D.2 Density Parameters

To see how the matter density parameter Ω_M scales with the redshift, consider its definition

$$\Omega_M(z) \equiv \frac{\rho(z)}{\rho_{\rm crit}(z)}, \tag{D3}$$

where the (physical) matter density $\rho(z)$ scales as $(1+z)^3$. Direct application of the latter yields

$$\Omega_M(z) = \frac{\rho_0(1+z)^3}{\rho_{\rm crit}(0)} \frac{\rho_{\rm crit}(0)}{\rho_{\rm crit}(z)}.$$

Identifying the components of this expression, we find

$$\Omega_M(z) = \frac{\Omega_M(0)}{E^2(z)}(1+z)^3. \tag{D4}$$

The treatment of Ω_Λ is analogous. If we assume a cosmological constant, the dark energy density will not scale with redshift, and we shall have

$$\Omega_\Lambda(z) = \frac{\Omega_\Lambda(0)}{E^2(z)}. \tag{D5}$$

D.3 The Cluster Over-Density at Virialization

For a flat universe in which $\Omega_M < 1$, the cluster over-density at the redshift $z_{\rm vir}$ of virialization, Δ_c, is approximated by the expression (Kitayama & Suto 1996)

$$\Delta_c \equiv \frac{\rho_{\rm vir}(z_{\rm vir})}{\bar{\rho}(z_{\rm vir})} \simeq 18\pi^2(1 + 0.4093\, w_f^{0.9052}), \tag{D6}$$

where

$$w_f \equiv \frac{1}{\Omega_f - 1}. \tag{D7}$$

Here, Ω_f is the the density parameter at virialization, given by

$$\Omega_f = \Omega_M \frac{(1+z_{\rm vir})^3}{E^2(z_{\rm vir})}. \tag{D8}$$

D.4 The Angular Diameter Distance

The angular diameter distance D_A at redshift z is given by

$$D_A = \frac{cZ(z)}{H_0} \frac{J([1-\Omega_{\rm tot}]Z^2(z))}{1+z}, \tag{D9}$$

where

$$J(x) = \begin{cases} \frac{\sin\sqrt{-x}}{\sqrt{-x}}, & x < 0; \\ \frac{\sin\sqrt{x}}{\sqrt{x}}, & x > 0; \\ 1 & x = 0, \end{cases}$$

and $1-\Omega_{\rm tot}$ is the curvature of space-time. Obviously, $J(x)=1$ in any critical (flat) universe. The function $Z(z)$ is the integral

$$Z=\int_{\frac{1}{1+z}}^{1}\frac{\mathrm{d}a}{a\sqrt{X}},$$

in which

$$X(a)=\frac{\Omega_M}{a}+\Omega_\Lambda a^2+(1-\Omega_M-\Omega_\Lambda).$$

Here, the density parameters are those at the present epoch, and the contribution from radiation to the total energy density of the universe has been disregarded.

E The Sheth-Tormen Mass Function

As a function of redshift, the cluster abundance in a mass interval $(M, M+\mathrm{d}M)$, expressed as the number of clusters per unit of comoving volume, is estimated by the expression

$$n(M,z)\mathrm{d}M=A\left(1+\frac{1}{\nu'^{2q}}\right)\sqrt{\frac{2}{\pi}}\frac{\bar{\rho}_0}{M}\frac{d\nu'}{dM}e^{-\frac{\nu'^2}{2}}\mathrm{d}M, \tag{E1}$$

where $\nu'=\sqrt{a}\nu$, $a=0.707$, $A\approx 0.322$ and $q=0.3$. $\bar{\rho}_0$ is the current background matter density of the universe, i.e. $\bar{\rho}_0=\rho_{\rm crit}\Omega_M(z=0)$. ν is given by

$$\nu=\frac{\delta_c}{D(z)\sigma(M)},$$

with $\delta_c\approx 1.69$ a dimensionless constant and

$$D(z)=\frac{g(z)}{g(0)(1+z)}.$$

Here, $g(z)$ is the suppression factor for linear growth, approximated by

$$g(z)\approx\frac{5}{2}\Omega_M[\Omega_M^{4/7}-\Omega_\Lambda+(1+\Omega_M/2)(1+\Omega_\Lambda/70)]^{-1}, \tag{E2}$$

where it is implicitly assumed that (see appendix D.2)

$$\Omega_M=\Omega_M(z),\ \ \Omega_\Lambda=\Omega_\Lambda(z).$$

$\sigma(M)$ is defined through

$$\sigma^2(R)=\frac{1}{2\pi^2}\int_0^\infty k^3P(k)\tilde{W}^2(kR)\frac{\mathrm{d}k}{k}, \tag{E3}$$

where R is related to M by

$$R(M)=\left(\frac{3M}{4\pi\bar{\rho}_0}\right)^{1/3}. \tag{E4}$$

The function $\tilde{W}(u)$ varies with $u \equiv kR$ as

$$\tilde{W}(u) = \frac{3(\sin u - u\cos u)}{u^3},$$

and the power spectrum $P(k)$ for the two-point correlation function is modeled using the relation $P \sim kT^2$, where

$$\begin{aligned} T(q) &= \frac{\log(1+2.34q)}{2.34q}[1+3.89q+(16.1q)^2+(5.46q)^3+(6.71q)^4]^{-1/4}; \\ q &\equiv \frac{k}{\Omega_M h^2 \mathrm{Mpc}^{-1}}. \end{aligned}$$

The normalization of σ is achieved by including the constant factor C in $P(k)$ such that

$$C^2 = \frac{\sigma_8}{\sigma(R = 8h^{-1}\mathrm{Mpc})}.$$

F Using the SZ Effect to Constrain H_0

The value of the Hubble constant has recently been constrained to 72 ± 8 km s^{-1} Mpc^{-1} using a combination of distance determinations based on observations of Cepheids (see Freedman et al. 2001). The Sunyaev-Zeldovich effect provides a way of constraining H_0 independently of the cosmic distance ladder. Although the shift of photons to higher frequencies caused by the SZ effect is essentially redshift independent, a combination of interferometric SZE observations and X-ray measurements of a galaxy cluster yields a measure of the angular diameter distance D_A (e.g. Holder et al. 2000), which can be compared to a separate measurement for the redshift. D_A is related to z and H_0 by

$$D_A = \frac{cZ(z)}{H_0}\frac{J([1-\Omega_{tot}]Z^2(z))}{1+z}, \tag{F1}$$

where $J(x) = 1$ for a flat cosmology ($Z(z)$ and $J(x)$ are defined in appendix D.4). The z dependence in D_A is shown for different cosmologies in figure 16, along with observed values of D_A and z from Reese et al. (2002).

A χ^2-fit to the numerical data gives $H_0 = 60 \pm 4$ km s^{-1} Mpc^{-1} (68 % confidence interval) for a ΛCDM cosmology with $\Omega_M = 0.3$ and $\Omega_\Lambda = 0.7$. The angular diameter distance is not quite as sensitive to the density parameters as to H_0. It is thus not suitable to attempt a fit to Ω_M or Ω_Λ.

Figure 16(b) clearly shows that the value $H_0 = 72 \pm 8$ km s^{-1} Mpc^{-1} provides a poor fit to the present data. It should be considered, however, that the gas distribution in clusters, if not uniform, could cause a severe underestimation of H_0 using the method described above (Carlstrom et al. 2000).

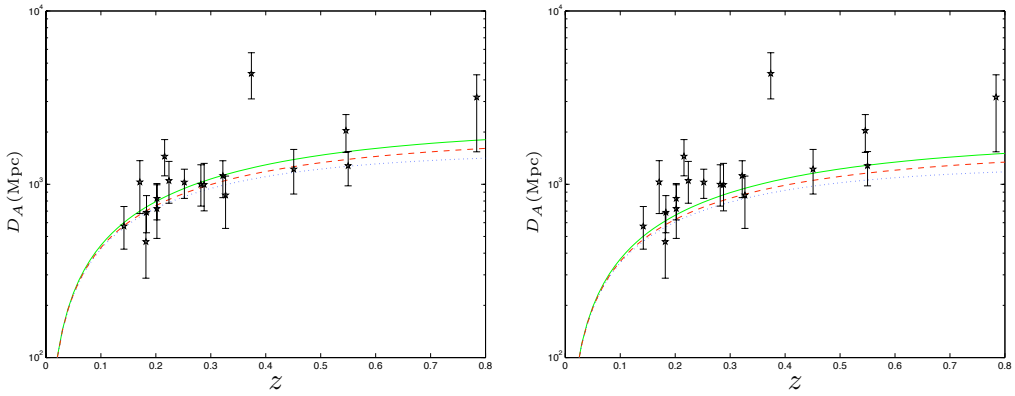

(a) $H_0 = 60$ km s^{-1} Mpc^{-1} (b) $H_0 = 72$ km s^{-1} Mpc^{-1}

Figure 16: $D_A(z)$ in different cosmological models. Solid lines represent the standard ΛCDM cosmology, dashed lines an open universe with $\Omega_M = 0.3$ and no dark energy and dotted lines a flat $\Omega_M = 1.0$ universe. Error bars show observations from Reese et al. (2002)

References

Aghanim N., Hansen S. H., Lagache G., 2004, arXiv:astro-ph/0402571

Allen S. W., Schmidt R. W., Fabian A. C., 2001, MNRAS 328, L37

Battistelli E. S., et al., 2002, ApJL 580, L101

Battye R. A., Weller J., 2003, Phys. Rev. D 68, 3506

Birkinshaw M., 1999, Phys. Reports 310, 97

Bryan G. L., Norman M. L., 1998, ApJ 495, 80

Carlstrom J. E. et al., 2000, in Particle Physics and the Universe, ed. L. Bergström, P. Carlson & C. Fransson (Singapore: World Scientific)

Carlstrom J. E., et al., 2002, ARA&A 40, 643

Diego J. M. et al., 2002, MNRAS 331, 556

Fabbri R., 1981, Ap&SS 77, 529

Fabbri R., et al., 1978, Ap&SS 59, 223

Fan Z., Chiueh T., 2001, ApJ 550, 547

Finoguenov A., Reiprich T. H., Böhringer H., 2001, A&A 368, 749

Freedman W. L., et al., 2001, ApJ 553, 47

Ge J., Bechtold J., Black J. H., 1997, ApJ 474, 67

Geisbüsch J., Kneissl R., Hobson M., 2004, arXiv:astro-ph/0406190

Holder G. P., 2004, ApJ 602, 18

Holder G. P., et al., 2000, ApJ 544, 629
Itoh N., Nozawa S., 2004, A&A 417, 827
Itoh N., et al., 1998, ApJ 502, 7
Jenkins A., et al., 2001, MNRAS 321, 372
Kay S. T., Liddle A. R., Thomas P. A., 2001, MNRAS 325, 835
Kitayama T., Suto Y., 1996, ApJ 469, 480
Kneissl R., et al., 2001, MNRAS 328, 783
Knop R. A., et al., 2003, ApJ 598, 102
Kompaneets A. S.,1956, Zh. E. F. T., 31, 876. Transl. in Sov. Phys. JETP 4, 730 (1957)
Lamarre J. M., et al., 2003, NewAR 47, 1017
LaRoque S. J., et al., 2002, AAS 200, 4105
Lima J. A. S., et al., 2000, MNRAS 312, 747
Lokas E. L., Bode P., Hoffman Y., 2004, MNRAS 349, 595
LoSecco J. M., Mathews G. J., Wang Y., 2001, Phys. Rev. D 64, 123002
Majumdar S., Mohr J. J., 2003, ApJ 586, 603
Markevitch M., et al., 1996, ApJ 456, 437
Mo H. J., White S. D. M., 2002, MNRAS 336, 112
Navarro J. F., Frenk C. S., White S. D. M., 1997, ApJ 490, 493
Peebles P. J. E., 1980, The Large-Scale Structure of the Universe, Princeton: Princeton U.P.
Perlmutter S., et al., 1999, ApJ 517, 565-586
Press W. H., Schechter P., 1974, ApJ 187, 425
Ratra B., Peebles P. J. E., 1988, Phys. Rev. D 37, 3407
Reed D., et al., 2003, MNRAS 346, 565
Reese E. D., et al., 2002, ApJ 581, 53
Rephaeli Y., 1980, ApJ 241, 858
Rephaeli Y., 1995, ApJ 445, 33
Rephaeli Y., Yankovitch D., 1997, ApJL 481, L55
Sandoval-Villalbazo A., García-Colín L. S., 2003, J. Phys. A: Math. Gen. 36, 4641
Sazonov S. Y., Sunyaev R. A., 1998a, Astron. Lett. 24, 643
Sazonov S. Y., Sunyaev R. A., 1998b, ApJ 508, 1
Schulz A. E., White M., 2003, ApJ 586, 723
Sheth R. K., Diaferio A., 2001, MNRAS 322, 901
Sheth R. K., Tormen G., 1999, MNRAS 308, 119
Sunyaev R. A., 1980, Sov. Astr. Lett. 6, 213
Sunyaev R. A., Zeldovich Y. B., 1970a, Ap&SS 7, 3

Sunyaev R. A., Zeldovich Y. B., 1970b, Ap&SS 7, 20
Sunyaev R. A., Zeldovich Y. B., 1972a, Astron. Astrophys. 20, 189
Sunyaev R. A., Zeldovich Y. B., 1972b, Comments Astrophys. Space Phys. 4, 173
Sunyaev R. A., Zeldovich Y. B., 1980a, MNRAS 190, 413
Sunyaev R. A., Zeldovich Y. B., 1980b, ARA&A 18, 537
Sunyaev R. A., Zeldovich Y. B., 1981, ASPRv 1, 1
Tang J., Fan Z., 2003, Chin. J. Astron. Astrophys. 3, 191
Viana P. T. P., Liddle A. R., 1999, MNRAS 303, 535
Wang L., Steinhardt P. J., 1998, ApJ 508, 483
Zeldovich Y. B., 1972, MNRAS 160, 1P
Zeldovich Y. B., Sunyaev R. A., 1969, Ap&SS 4, 301
Zeldovich Y. B., Sunyaev R. A., 1980a, Sov. Astr. Lett. 6, 285 (1981)
Zeldovich Y. B., Sunyaev R. A., 1980b, Sov. Astr. Lett. 6, No. 6 (1981)